Int. J. Heat Mass Transfer. Vol. 32, No. 10, pp. 1939–1954, 1989
Printed in Great Britain

0017-9310/89 $3.00+0.00

The effect of the direction of the external magnetic field on the three-dimensional natural convection in a cubical enclosure

HIROYUKI OZOE and KAZUTO OKADA
Institute of Advanced Material Study, Kyushu University, Kasuga, Fukuoka, Japan

(*Received* 20 *February* 1989)

Abstract—Three-dimensional conservation equations for natural convection in a cubic enclosure heated from one side wall and cooled from an opposing wall are numerically solved under three different external magnetic fields either in the X-, Y- or Z-directions. Sample computations are carried out for $Ra = 10^6$ and 10^7 and $Ha = 0$–500 for $Pr = 0.054$. The external magnetic field perpendicular to the vertical boundary layer type flow is found to be most effective in suppressing the convection. However, the external magnetic field parallel to the vertical hot and cold walls is found to be least effective, although it is perpendicular to the main circulating flow along both the vertical and horizontal boundaries. When the magnetic field is relatively strengthened, for example, at $Ra = 10^6$ and $Ha = 300$, secondary flow is found to be doubly strengthened with a reduction in the main circulation flow.

1. INTRODUCTION

ELECTRO-CONDUCTING fluid has been increasingly used in the manufacturing process of semi-conducting material such as silicon crystal or gallium arsenide. In the Czochralski method, the polycrystal silicon is melted in a crucible and pulled up from the liquid surface to produce a purified single crystal rod. In this operation, both a crucible and a crystal rod are rotated in the same or reverse directions. The melted silicon in a crucible convects in a gravitational field due to the temperature difference between the crucible and the rod. In this process, the addition of an external magnetic field has been reported to be quite effective in controlling the convection in a crucible [1]. Between the crucible and the rotating rod, there is a free surface and the surface tension also affects the convection. The combination of these external forces makes it difficult to predict the bulk convection in a crucible a priori intuitively. This is especially true for the general three-dimensional convection field. Some of the previous works, Hunt and Wilks [2], Nagase *et al.* [3], Tabeling [4], Raptis and Vlahos [5], Maekawa and Tanasawa [6], Munakata and Tanasawa [7], Weiss [8], and Ozoe and Maruo [9] studied the convection of liquid metal with magnetic forces but were limited to either boundary layer, two-dimensional or linear theory. Mihelcic *et al.* [10] reported the three-dimensional simulation of the Czochralski bulk flow but did not include a magnetic field. The effect of the direction of the external magnetic field has apparently not yet been reported. Maekawa and Tanasawa [11] studied the effect of the direction of the magnetic field in general but limited it to a two-dimensional field.

In this paper, the effect of the direction of the external magnetic field on the natural convection of molten silicon in a cubical enclosure was studied numerically with three-dimensional Navier–Stokes equation including Lorentz force terms.

2. MATHEMATICAL MODEL

2.1. *The systems considered*

The systems considered in this paper are shown schematically in Fig. 1. The fluid in a cubic enclosure is heated from a vertical side wall and cooled from an opposing vertical wall. The other four walls are thermally insulated. The direction of gravity is along the Z-axis. The external magnetic field Bx is added only from the X-direction for the system shown in Fig. 1(a). The fluid in this enclosure receives both the buoyancy force resulting from heat transfer through side walls and the Lorentz force resulting from the convection of fluid in an external magnetic field. The system with an external magnetic field in the Y-direction only as shown in Fig. 1(b) and that in the Z-direction only as in Fig. 1(c) are also considered in this paper so that the effect of the direction of the external magnetic field is expected to be compared with each other.

2.2. *Model equations*

The model equations consist of mass balance, energy balance, momentum balance and the state equation for fluid. The convection of electro-conducting fluid receives the Lorentz force in a magnetic field and these terms should be included in momentum equations.

The Lorentz force term $\mathbf{F}$ is given as follows [9]:

$$\mathbf{F} = \rho_e \mathbf{E} + \mathbf{J} \times \mathbf{B} \tag{1}$$

NOMENCLATURE

B magnetic induction (magnetic field) [Wb m^{-2}, V s m^{-2}]
B_0 external magnetic field [Wb m^{-2}]
C specific heat [J kg^{-1} K^{-1}]
D electric displacement [C m^{-2}]
E electric field intensity [V m^{-1}, N C^{-1}]
e unit vector for an external magnetic field [—]
F Lorentz force [N m^{-3}]
g acceleration due to gravity [m s^{-2}]
Gr Grashof number, $g\beta(\theta_h-\theta_c)l^3/\nu^2$ [—]
Ha Hartman number, $(\sigma_e/(\rho\nu))^{1/2}B_0 l$ [—]
J electric current density [A m^{-2}]
k thermal conductivity of fluid [J m^{-1} s^{-1} K^{-1}]
L $l/x_0 = Ra^{1/3}$ [—]
l distance between hot and cold walls [m]
Nu average Nusselt number, $ql/[k(\theta_h-\theta_c)]$
Pr Prandtl number, ν/α [—]
q heat flux density [J m^{-2} s^{-1}]
Ra Rayleigh number, $Gr\ Pr$ [—]
T dimensionless temperature $(\theta-\theta_0)/(\theta_h-\theta_c)$ [—]
t time [s]
U dimensionless velocity vector [—]
u velocity vector [m^2 s^{-1}]
u x-component of velocity [m s^{-1}]
U u/u_0 [—]
v y-component of velocity [m s^{-1}]
V v/v_0 [—]
w z-component of velocity [m s^{-1}]
W w/w_0 [—]
x coordinate [m]
X x/x_0 [—]
y coordinate [m]
Y y/y_0 [—]
z coordinate [m]
Z z/z_0 [—].

Greek symbols

α thermal diffusivity of fluid [m^2 s^{-1}]
β volumetric coefficient of expansion [K^{-1}]
ε dielectric constant [C V^{-1} m^{-1}]
θ temperature [K]
θ_c cold wall temperature [K]
θ_h hot wall temperature [K]
μ viscosity of fluid [kg m^{-1} s^{-1}]
ν kinematic viscosity [m^2 s^{-1}]
$\boldsymbol{\xi}$ vorticity vector [s^{-1}]
ρ density of fluid [kg m^{-3}]
ρ_e electric charge density of fluid [C m^{-3}]
σ_e electric conductivity of fluid [Ω^{-1} m^{-1}]
τ dimensionless time, t/t_0
$\boldsymbol{\psi}$ vector potential for a flow field [m^2 s^{-1}]
ψ_e scalar potential for an electric field [Wb s^{-1}, V]
$\boldsymbol{\Psi}$ dimensionless vector potential for a flow field, $\boldsymbol{\psi}/\alpha$
Ψ_e dimensionless scalar potential for an electric field, ψ_e/ψ_{e0}
$\boldsymbol{\Omega}$ dimensionless vorticity vector, $\boldsymbol{\xi}/(\alpha x_0^{-2})$.

Operators

$D/D\tau$ $\partial/\partial\tau + U\partial/\partial X + V\partial/\partial Y + W\partial/\partial Z$
∇^2 $\partial^2/\partial X^2 + \partial^2/\partial Y^2 + \partial^2/\partial Z^2$
∇ $(\partial/\partial X, \partial/\partial Y, \partial/\partial Z)$
$\times$ vector product.

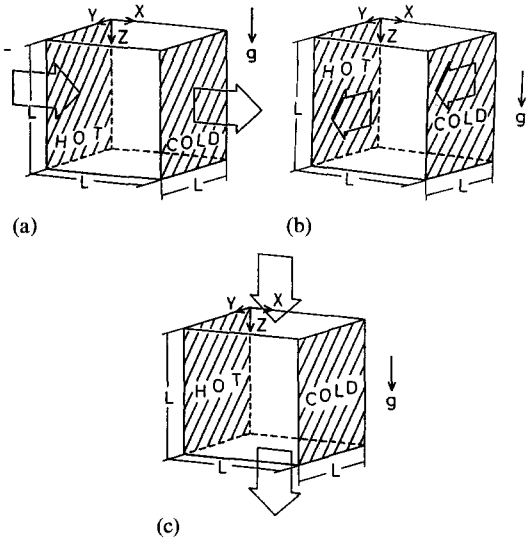

FIG. 1. Schematics of the system: (a) external magnetic field in the X-direction only; (b) external magnetic field in the Y-direction only; (c) external magnetic field in the Z-direction only.

where ρ_e is the electric charge density of fluid, **E** the electric field intensity, **J** the electric current density and **B** the magnetic field.

The Maxwell equation for a magneto-electric field gives

$$\text{div}\ \mathbf{D} = \rho_e \tag{2}$$

where **D** is the electric displacement and is related to **E** as follows:

$$\mathbf{D} = \varepsilon\mathbf{E} \tag{3}$$

where ε is a dielectric constant. On the other hand, Ohm's law holds for this system

$$\mathbf{J} = \rho_e\mathbf{u} + \sigma_e(\mathbf{E} + \mathbf{u}\times\mathbf{B}) \tag{4}$$

where σ_e is the electric conductivity and **u** the fluid velocity vector. In this electro-magnetic field, the high frequency wave such as light is not treated and the displacement current is zero

$$\partial\mathbf{D}/\partial t = 0. \tag{5}$$

The fluid is also assumed to be electrically neutral

and the convective term $\rho_e \mathbf{u}$ is neglected in Ohm's equation. Then equations (1) and (4) become

$$\mathbf{F} = \mathbf{J} \times \mathbf{B} \tag{6}$$

$$\mathbf{J} = \sigma_e(\mathbf{E} + \mathbf{u} \times \mathbf{B}). \tag{7}$$

Following Kobayashi [12], a scalar potential for an electric field is now introduced as follows:

$$\mathbf{E} = -\nabla \psi_e. \tag{8}$$

Then we have

$$\mathbf{J} = \sigma_e(-\nabla \psi_e + \mathbf{u} \times \mathbf{B}). \tag{9}$$

The equation of continuity for electric current $\mathbf{J}$ gives

$$\nabla \cdot \mathbf{J} = 0. \tag{10}$$

Equations (9) and (10) give

$$\nabla^2 \psi_e = \nabla \cdot (\mathbf{u} \times \mathbf{B}) \tag{11}$$

where the electric conductivity σ_e is constant. Equations (6) and (9) give

$$\mathbf{F} = -\sigma_e \nabla \psi_e \times \mathbf{B} + \sigma_e(\mathbf{u} \times \mathbf{B}) \times \mathbf{B}. \tag{12}$$

Under any specific external magnetic field $\mathbf{B}$, equation (11) gives the electric scalar potential ψ_e. Both ψ_e and the magnetic field $\mathbf{B}$ give a Lorentz force from equation (12).

The system equations are summarized in dimensionless form as follows. They are an energy equation and a vorticity equation

$$\mathrm{D}T/\mathrm{D}\tau = \nabla^2 T \tag{13}$$

$$\begin{aligned} \mathrm{D}\boldsymbol{\Omega}/\mathrm{D}\tau = {} & (\boldsymbol{\Omega} \cdot \nabla)\mathbf{U} + Pr \nabla^2 \boldsymbol{\Omega} \\ & + Pr(-\partial T/\partial Y, \partial T/\partial X, 0)^{\mathrm{T}} \\ & + Ha^2 Ra^{-2/3} Pr\{-\nabla \times (\nabla \Psi_e \times \mathbf{e}) \\ & + \nabla \times [(\mathbf{U} \times \mathbf{e}) \times \mathbf{e}]\}. \end{aligned} \tag{14}$$

The vorticity for the flow field is related to the vector potential for the flow field as follows:

$$\boldsymbol{\Omega} = -\nabla^2 \boldsymbol{\Psi}. \tag{15}$$

The vector potential $\boldsymbol{\Psi}$ is related to the velocity vector as follows:

$$\mathbf{U} = \nabla \times \boldsymbol{\Psi}. \tag{16}$$

The scalar potential for an electric field is rewritten as

$$\nabla^2 \Psi_e = (\nabla \times \mathbf{U}) \cdot \mathbf{e}. \tag{17}$$

In the above equations, $\mathbf{e}$ represents a unit vector in the direction of the external magnetic field.

The dimensionless variables are defined as

$$X = x/x_0, \quad Y = y/y_0, \quad Z = z/z_0, \quad U = u/u_0, \quad V = v/v_0,$$

$$W = w/w_0, \quad \tau = t/t_0, \quad \Psi_e = \psi_e/\psi_{e0}, \quad \boldsymbol{\Psi} = \boldsymbol{\psi}/\alpha,$$

$$L = l/x_0 = Ra^{1/3}, \quad Pr = \nu/\alpha, \quad T = (\theta - \theta_0)/(\theta_h - \theta_c),$$

$$Ra = g\beta(\theta_h - \theta_c)l^3/(\alpha\nu), \quad Ha = [\sigma_e/(\rho\nu)]^{1/2} B_0 l,$$

$$x_0 = y_0 = z_0 = [g\beta(\theta_h - \theta_c)/(\alpha\nu)]^{-1/3}, \quad t_0 = x_0^2/\alpha,$$

$$u_0 = v_0 = w_0 = \alpha/x_0, \quad \theta_0 = (\theta_h + \theta_c)/2, \quad \psi_{e0} = \alpha B_0.$$

2.3. *The initial and boundary conditions*

Numerical computation for three-dimensional turbulent natural convection in a cubical enclosure for air was carried out in ref. [13]. Following the scheme in ref. [13], the laminar natural convection was computed for low Prandtl number fluid in this work. It supplied an initial stable convection state.

The boundary conditions for this system are given as follows for all variables on all six walls of a cubical enclosure.

Temperature

$$T = 0.5 \quad \text{at} \quad X = 0$$

$$T = -0.5 \quad \text{at} \quad X = L$$

$$\partial T/\partial Y = 0 \quad \text{at} \quad Y = 0 \quad \text{and} \quad L$$

$$\partial T/\partial Z = 0 \quad \text{at} \quad Z = 0 \quad \text{and} \quad L.$$

Velocity

$$U = V = W = 0 \quad \text{at} \quad X = 0 \quad \text{and} \quad L$$

$$Y = 0 \quad \text{and} \quad L$$

$$Z = 0 \quad \text{and} \quad L.$$

Vector potential

$$\partial \Psi_x/\partial X = \Psi_y = \Psi_z = 0 \quad \text{at} \quad X = 0 \quad \text{and} \quad L$$

$$\Psi_x = \partial \Psi_y/\partial Y = \Psi_z = 0 \quad \text{at} \quad Y = 0 \quad \text{and} \quad L$$

$$\Psi_x = \Psi_y = \partial \Psi_z/\partial Z = 0 \quad \text{at} \quad Z = 0 \quad \text{and} \quad L.$$

Vorticity

$$\Omega_x = 0, \quad \Omega_y = -\partial W/\partial X,$$

$$\Omega_z = \partial V/\partial X \quad \text{at} \quad X = 0 \quad \text{and} \quad L$$

$$\Omega_x = \partial W/\partial Y, \quad \Omega_y = 0,$$

$$\Omega_z = -\partial U/\partial Y \quad \text{at} \quad Y = 0 \quad \text{and} \quad L$$

$$\Omega_x = -\partial V/\partial Z, \quad \Omega_y = \partial U/\partial Z,$$

$$\Omega_z = 0 \quad \text{at} \quad Z = 0 \quad \text{and} \quad L.$$

Scalar potential for an electric field

$$\partial \Psi_e/\partial X = 0 \quad \text{at} \quad X = 0 \quad \text{and} \quad L$$

$$\partial \Psi_e/\partial Y = 0 \quad \text{at} \quad Y = 0 \quad \text{and} \quad L$$

$$\partial \Psi_e/\partial Z = 0 \quad \text{at} \quad Z = 0 \quad \text{and} \quad L.$$

The boundary conditions for vector potential are given by Hirasaki and Hellums [14]. The vorticity boundary conditions are from zero velocity conditions on the walls. The electrical insulation on the walls give the boundary conditions for scalar potential for an electric field.

The cubical enclosure was divided into unequal grids as shown in Fig. 2. There are 21 grids in the X-direction, 11 in the Y-direction and 15 in the Z-direction. The grid locations are listed in Table 1.

The computational scheme is the ADI method and is similar to that of ref. [9].

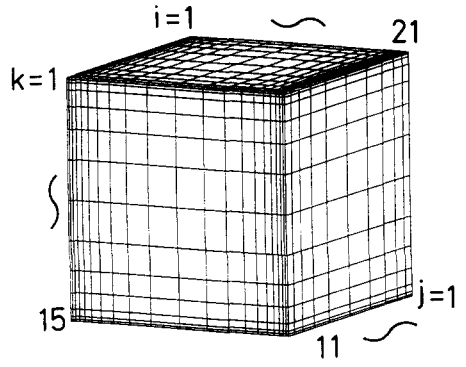

FIG. 2. Grid divisions of the enclosure considered.

Table 1. Coordinates of grid points

Grid	X-Coordinate	Y-Coordinate	Z-Coordinate
1	0.00000E+00	0.00000E+00	0.00000E+00
2	0.10000E−01	0.50000E−01	0.80000E−02
3	0.23320E−01	0.11762	0.20000E−01
4	0.41070E−01	0.20907	0.50000E−01
5	0.64720E−01	0.33274	0.11762
6	0.96220E−01	0.50000	0.20907
7	0.13818	0.66726	0.33274
8	0.19409	0.79093	0.50000
9	0.26857	0.88238	0.66726
10	0.36780	0.95000	0.79093
11	0.50000	1.0000	0.88238
12	0.63220		0.95000
13	0.73143		0.98000
14	0.80591		0.99200
15	0.86182		1.0000
16	0.90378		
17	0.93528		
18	0.95893		
19	0.97668		
20	0.99000		
21	1.0000		

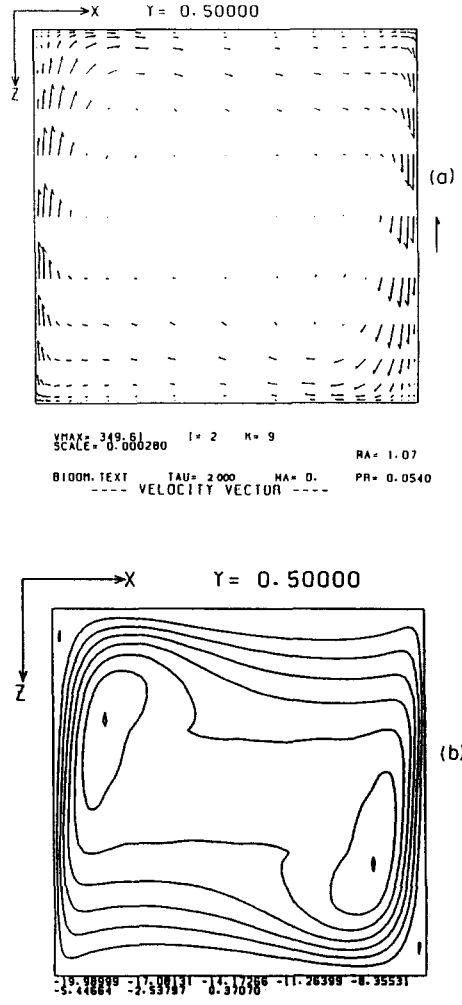

FIG. 3. Computed results at $Ra = 10^7$ and $Pr = 0.054$: (a) velocity vectors at $Y = 0.5$; (b) contour maps of vector potential Ψ_y at $Y = 0.5$ with a minimum value of -19.99.

3. COMPUTED RESULTS

3.1. *Natural convection of low Prandtl number fluid*

The initial condition for this computation is a static state and is isothermal at an average temperature at all internal fluid regimes. Computations were carried out for molten silicon ($Pr = 0.054$). However, the computations are expected to be equally possible for smaller Prandtl number fluids.

The converged convection at $Ra = 10^7$, $Pr = 0.054$ is shown in the velocity profile at $Y = 0.5$ in Fig. 3(a) and in the Y-component of the vector potential at the $Y = 0.5$ plane in Fig. 3(b). The Y-component of the vector potential is a major component and the maximum value is -19.99. In Fig. 4, the isothermal contour maps are shown in three different cross sections at the middle height of the enclosure. Figure 4(b) represents that at $Y = 0.5$ in which temperature stratification is apparent in a core regime even at this high Grashof number $Gr = 1.85 \times 10^8$ for this fluid at a low Prandtl number $Pr = 0.054$. In Fig. 4(a) the thermal boundary layer is established over the hot (left) and cold (right) walls. The thermal boundary layer shows a slight wavy shape and gets thicker near the insulated side walls. This is because the major circulating convection rate is decreased near the rigid side walls at $Y = 0$ and L. Figure 5 shows the perspective view of the whole velocity vectors at $Ra = 10^6$ and $Pr = 0.054$. These show a quasi two-dimensional natural convection in the cubic regime.

3.2. *Natural convection in a magnetic field*

The initial condition is the convective state obtained for a non-magnetic field described above.

Figure 6 shows the response curves of the Y-component of a vector potential after a step addition of a magnetic field. Curves (1)–(3) are the X-, Y- or Z-direction of an external magnetic field. They are all at $Ra = 10^7$, $Ha = 100$ and $Pr = 0.054$. Curve (2) is not at a completely converged state because it required extremely small time steps for a numerical stability. Table 2 summarizes the computed results. The average

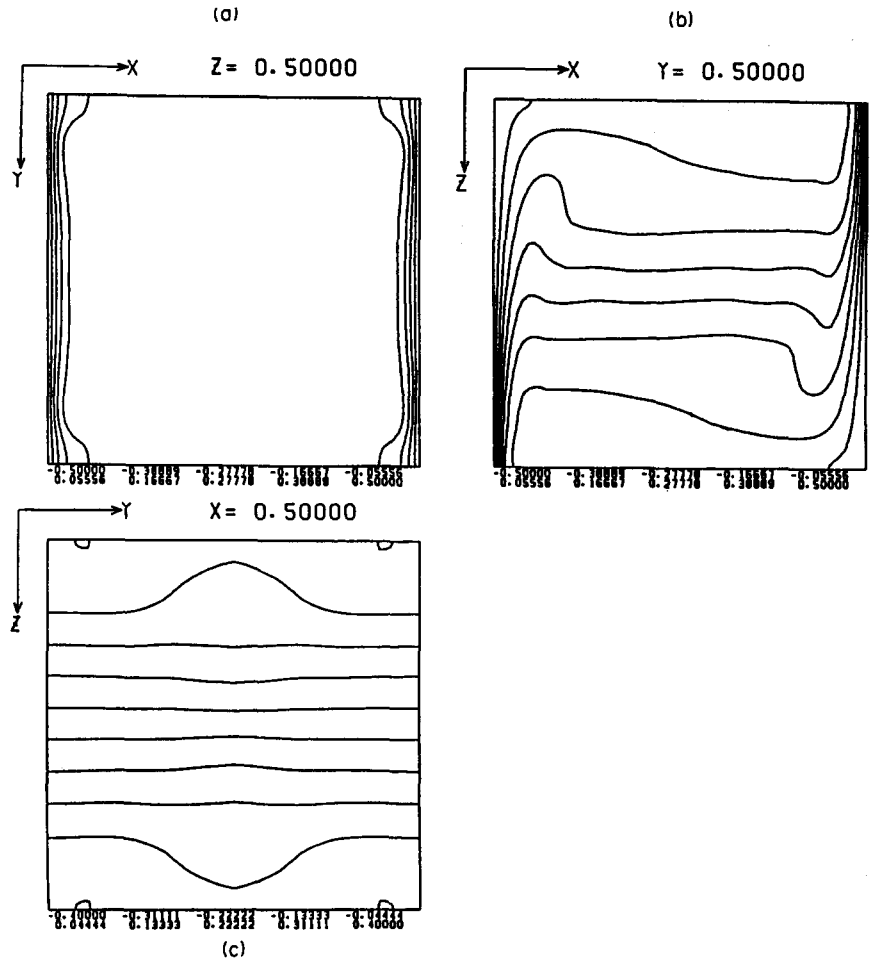

FIG. 4. Computed isotherms at $Ra = 10^7$ and $Pr = 0.054$: (a) $Z = 0.5$; (b) $Y = 0.5$; (c) $X = 0.5$.

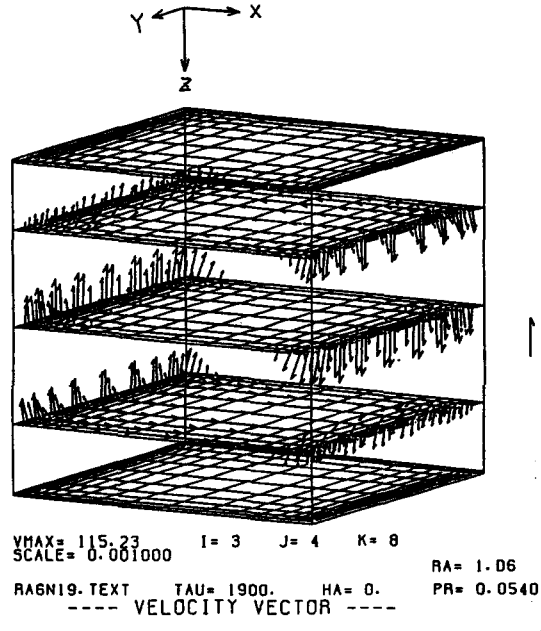

FIG. 5. Perspective view of the velocity vectors at $Ra = 10^6$ and $Pr = 0.054$.

Table 2. Summary of the computed results

Ra	Ha	B	Nu	Ψ_y(center)
10^7	0	—	10.524	−15.708
10^7	100	X	9.655	−13.682
10^7	100	Y	10.445	−15.523
10^7	100	Z	10.024	−14.805
10^6	0	—	5.7371	−8.876
10^6	100	X	4.4577	−7.792
10^6	200	X	2.9168	−4.670
10^6	300	X	2.2508	−2.998

Nusselt numbers are slightly different from each other under this weak magnetic field. However, the difference is apparent. The magnetic field in the X-direction gave the smallest value of the average Nusselt number on the vertical hot wall. The magnetic field in the Y-direction gave the largest. The central value of the Y-component of the vector potential also gave the same order of decrease in their magnitudes. This represents that the heat transfer is convection dominated at this condition even for the fluid at this low Prandtl number of 0.054.

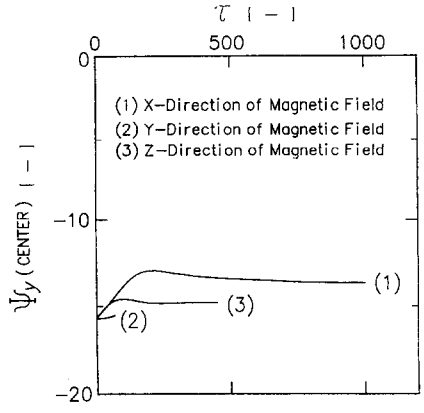

FIG. 6. Transient responses of the central value of the Y-component of the vector potential at $Ra = 10^7$, $Pr = 0.054$ and $Ha = 100$: (1) external magnetic field in the X-direction; (2) external magnetic field in the Y-direction; (3) external magnetic field in the Z-direction.

It is commonly accepted that the external magnetic field suppresses the flow most effectively when the magnetic field is imposed perpendicular to the direction of the flow of electro-conducting fluid.

When the external magnetic field is in the Y-direction, the magnetic field is perpendicular to both the vertical boundary layer flow along the hot or cold plates and the horizontal flow along the ceiling and the bottom adiabatic plates; major circulating convection. The authors expected to have the most significant suppression for this external magnetic field in the Y-direction. The results were just the opposite. The magnitude of the Lorentz force term was therefore computed term by term. In the momentum equation in the Z-direction (and also in the Y-component of the vorticity equation), the terms $\partial\Psi_e/\partial Y - W$ represent the Lorentz force when the external magnetic field is in the X-direction only. The terms $-\partial\Psi_e/\partial X - W$ become the Lorentz force when the external magnetic field is in the Y-direction only. The magnitude of these terms is shown in Fig. 7. When the magnetic field in the X-direction is given, the $\partial\Psi_e/\partial Y$ term is small but the $-W$ term is large along the vertical walls and the resulting magnitude of the Lorentz force is large along the hot and cold vertical walls.

When the magnetic field in the Y-direction is exerted, both the $-\partial\Psi_e/\partial X$ term and the $-W$ term have a large magnitude along the vertical heated boundaries but with opposite signs so they cancel each other out to produce a Lorentz force with a small magnitude in the momentum equation in the Z-direction. This appears to be the reason why the Y-magnetic field gave the unexpectedly small suppression effect.

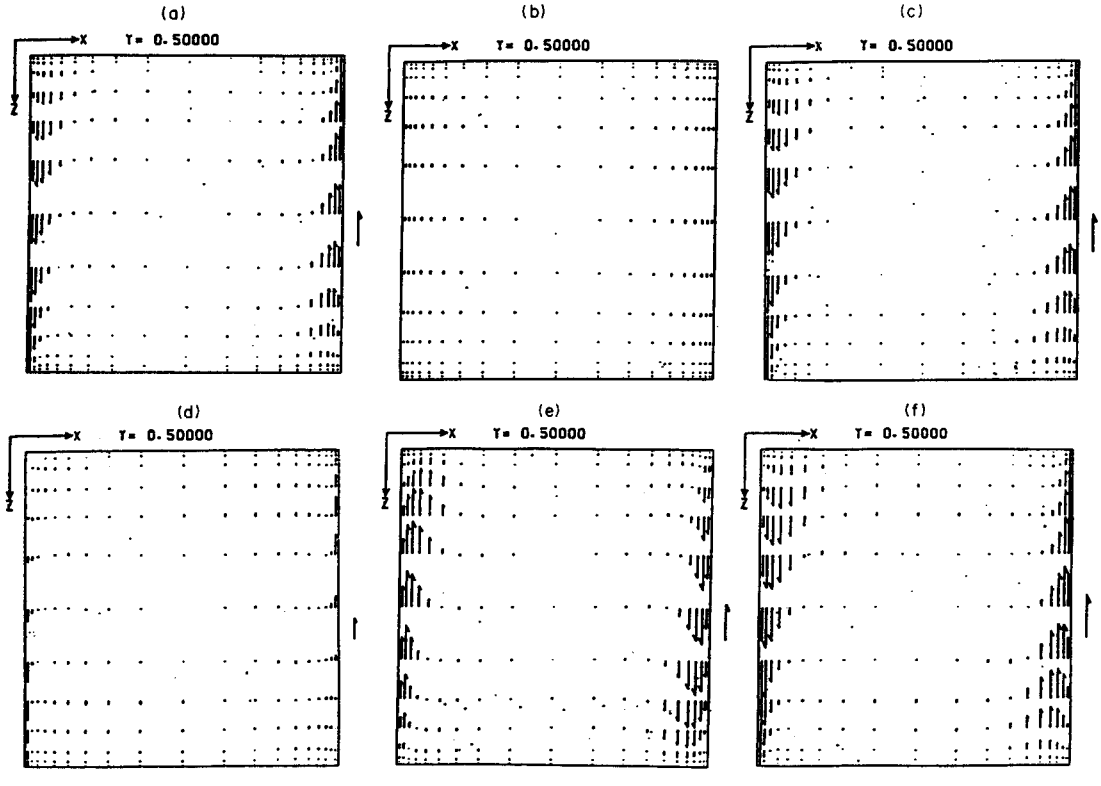

FIG. 7. Graphical presentation of the magnitude of the Lorentz force for two cases of an external magnetic field in the X-direction only or in the Y-direction only: (a)–(c) are for the magnetic field in the X-direction; (d)–(f) are for the magnetic field in the Y-direction. (a) $\partial\Psi_e/\partial Y - W$; (b) $\partial\Psi_e/\partial Y$; (c) $-W$; (d) $-\partial\Psi_e/\partial X - W$; (e) $-\partial\Psi_e/\partial X$; (f) $-W$.

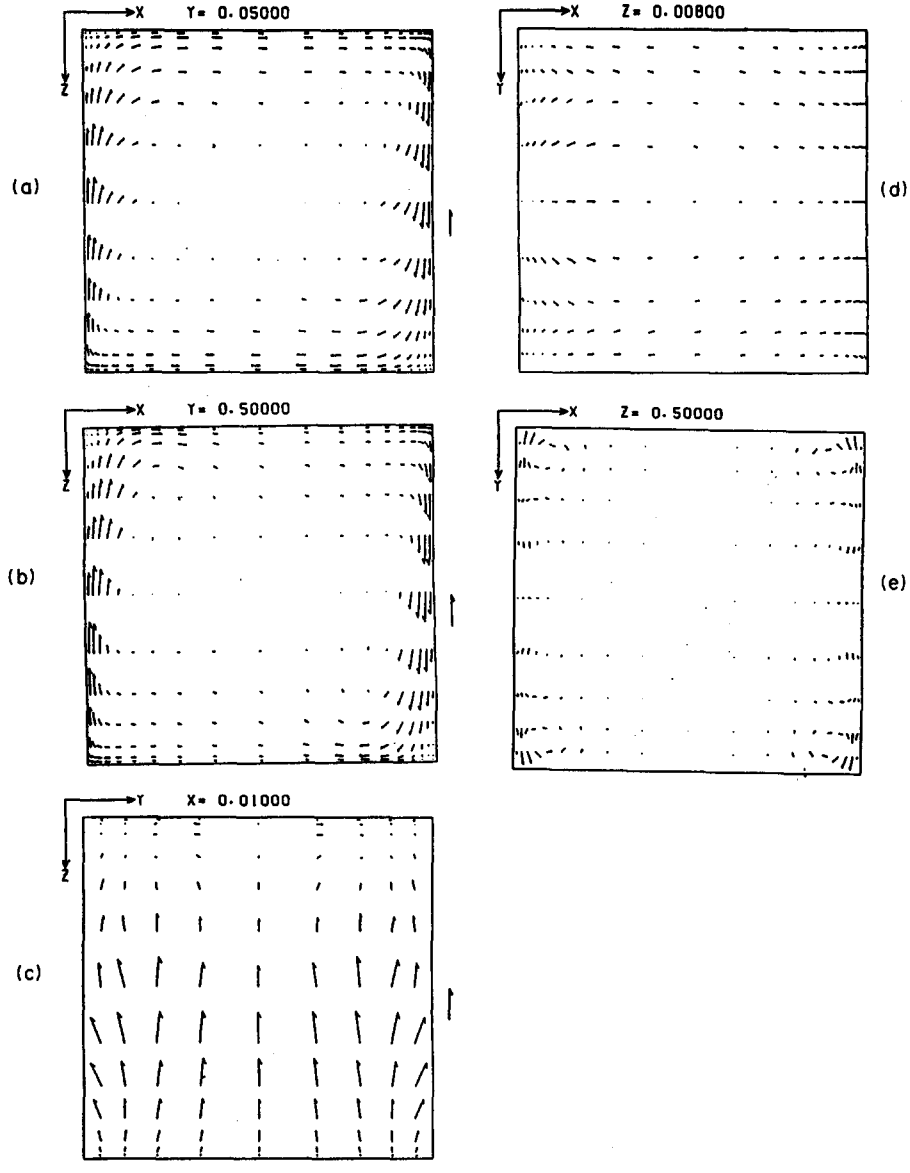

FIG. 8. Computed velocity vectors at various cross sections at $Ra = 10^7$, $Ha = 100$ and $Pr = 0.054$ under a magnetic field in the Z-direction at: (a) $Y = 0.05$; (b) $Y = 0.5$; (c) $X = 0.01$; (d) $Z = 0.008$; (e) $Z = 0.5$.

Figure 8 shows the velocity profiles in various cross sections. These are similar to other cases and only the system under the Z-directional magnetic field is shown herein at $Ra = 10^7$ and $Pr = 0.054$.

Table 2 also includes the converged solutions for various Hartman numbers under an external magnetic field in the X-direction for $Ra = 10^6$ and $Pr = 0.054$. The average Nusselt number is decreased extensively when the Hartman number is raised stepwise and an almost conductive state was attained at $Ha = 500$.

The isotherms at $Ra = 10^6$ and $Pr = 0.054$ are shown in Fig. 9. The isotherms at the cross section of $Y = 0.5$ represent the effect of the magnetic field in the X-direction. The thermal boundary layer thickness spreads into the core regime as seen at the cross section at $Z = 0.5$.

Figure 10 shows the contours of the Y-component of the vector potential. The ascending and descending flows in Fig. 10(c) are suppressed by the horizontal magnetic field in the X-direction and the vertical boundary layer apparently disappeared as seen in Fig. 10(f) at the plane, $Y = 0.5$. The magnetic field suppresses the convective flow which is perpendicular to its field.

The contour maps of the X-component of the vector potential are shown in Fig. 11. It has the maximum value of 1.63 when there is no magnetic field. On the other hand when $Ha = 300$, the maximum value increases to 3.69 in the cross section at $X = 0.065$. This suggests that the external magnetic field suppresses the major circulation with an increase in the strength of a secondary flow. This phenomenon may not have

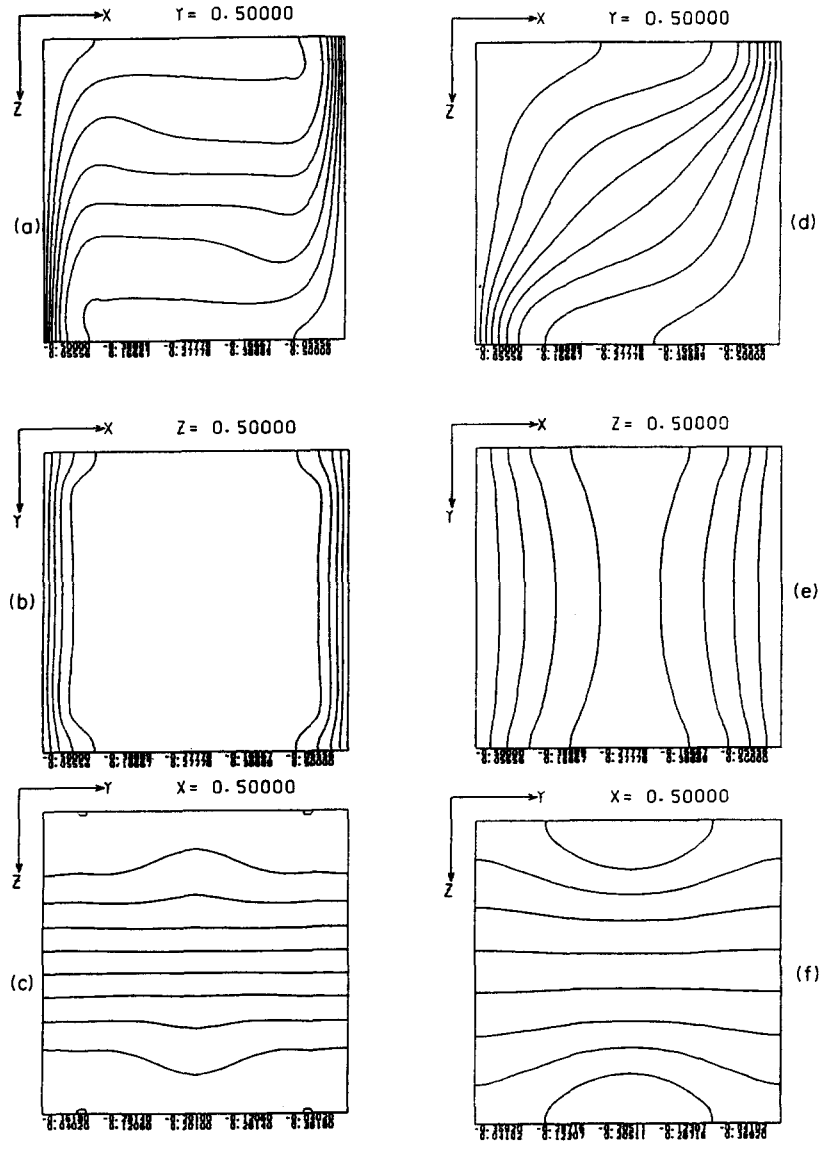

FIG. 9. Computed isotherms at $Ra = 10^6$ and $Pr = 0.054$: (a)–(c) are for $Ha = 0$; (d)–(f) are for $Ha = 300$. (a) and (d) are at $Y = 0.5$; (b) and (e) are at $Z = 0.5$; (c) and (f) are at $X = 0.5$.

been stated explicitly so far on the effect of the magnetic field in a three-dimensional field.

The effect of the external magnetic field in the X-direction can be seen more clearly in Fig. 12. The velocity profiles in the cross section at $Y = 0.5$ are shown for $Ha = 0$–500. The decrease in the magnitude of the main circulation is apparent. The flow profile dramatically changed. The vertical boundary layer disappeared while the horizontal velocity components near the upper and lower boundaries are affected less.

The velocity profiles in the cross section very near the heated walls are interesting to note as shown in Fig. 13. At the upper left- and right-hand corners, the velocity vectors along the top plane appear to be diverging at these corners. The same velocity appears along the lower corners near the cold wall because of the symmetry of the condition. This flow mode does not exist at $Ha = 0$. This peculiar characteristic is apparently due to the magnetic forces in a three-dimensional domain. Even this flow dies out at $Ha = 500$ as seen in Fig. 13(e).

These can be seen also in the perspective views of the velocity vectors as shown in Fig. 14 at various Hartman numbers.

3.3. *Natural convection under very strong magnetic field*

At $Ha = 500$ with the magnetic field in the X-direction, the Lorentz force appears to be strong enough to stop the convection essentially. The isotherms in Fig. 15 at the cross section at $Y = 0.5$ shows tilted isotherms in the core regime which suggest the dominance in the conductive heat transfer. The isotherms are almost at an equal distance as seen in three per-

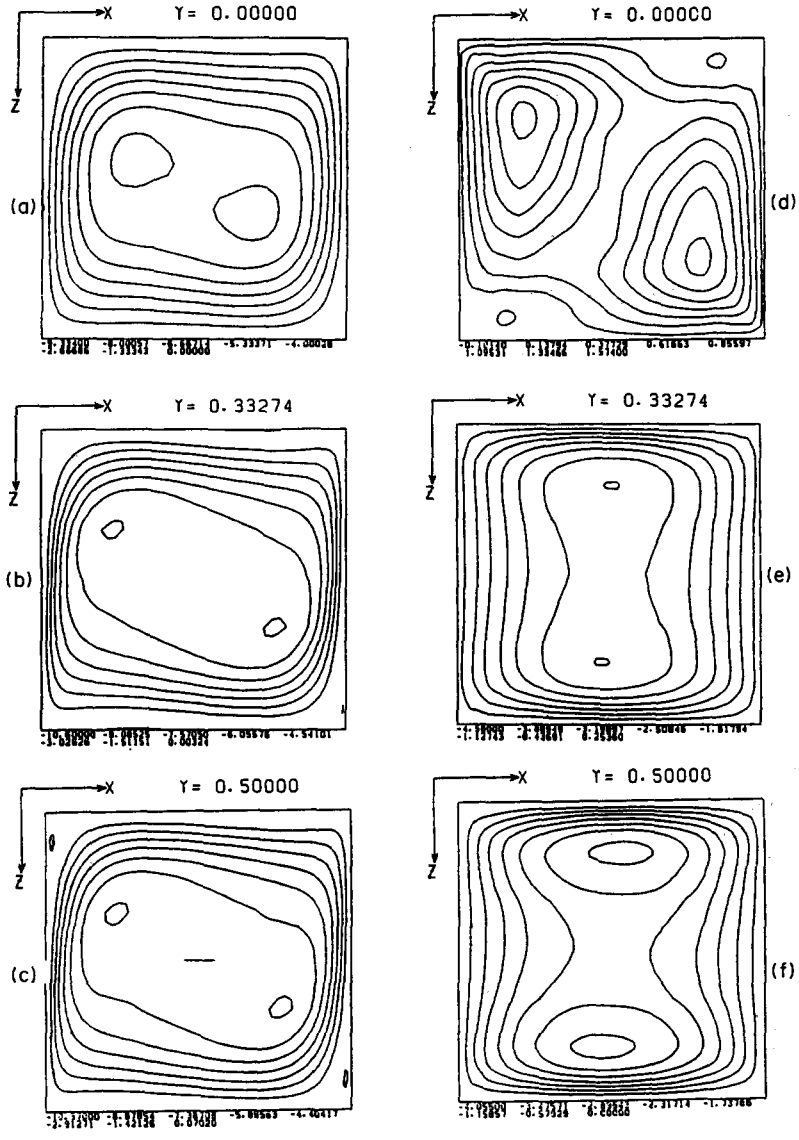

FIG. 10. Contour maps of vector potential Ψ_y at $Ra = 10^6$ and $Pr = 0.054$: (a) at $Ha = 0$ and $Y = 0$; (b) at $Ha = 0$ and $Y = 0.33$; (c) at $Ha = 0$ and $Y = 0.5$; (d) at $Ha = 300$ and $Y = 0$; (e) at $Ha = 300$ and $Y = 0.33$; (f) at $Ha = 300$ and $Y = 0.5$.

pendicular cross sections through the center of the regime.

In Fig. 16, the contour maps of the Y-component of the vector potential are shown at various cross sections of the constant Y plane under the magnetic field in the Y-direction at $Ha = 500$ and $Ra = 10^6$. The flow field consists of the outer circulating regime and multiple closed convection cells in a core regime. The vertical flow is suppressed but the horizontal (parallel to the X-magnetic field) velocity component is not suppressed and maintains a similar magnitude along the upper and lower boundaries. The ascending and descending flows are very weak and they fill the whole horizontal cross section in a core regime under this horizontal magnetic field in the X-direction.

4. SUMMARY OF THE RESULTS

The three-dimensional mathematical model for natural convection in a cubic enclosure heated from one side wall and cooled from an opposing wall and under an external magnetic field was presented as well as the boundary conditions for all variables. The finite difference scheme was developed and the stable solutions were obtained for $Ra = 10^6$ and 10^7 and $Ha = 0$–500 at $Pr = 0.054$ (molten silicon). The ascending and descending boundary layer type flows along the heated and cooled walls were mostly suppressed by the horizontal external magnetic field (X-direction) perpendicular to the heated vertical wall. However, the magnetic field (Y-direction) horizontal

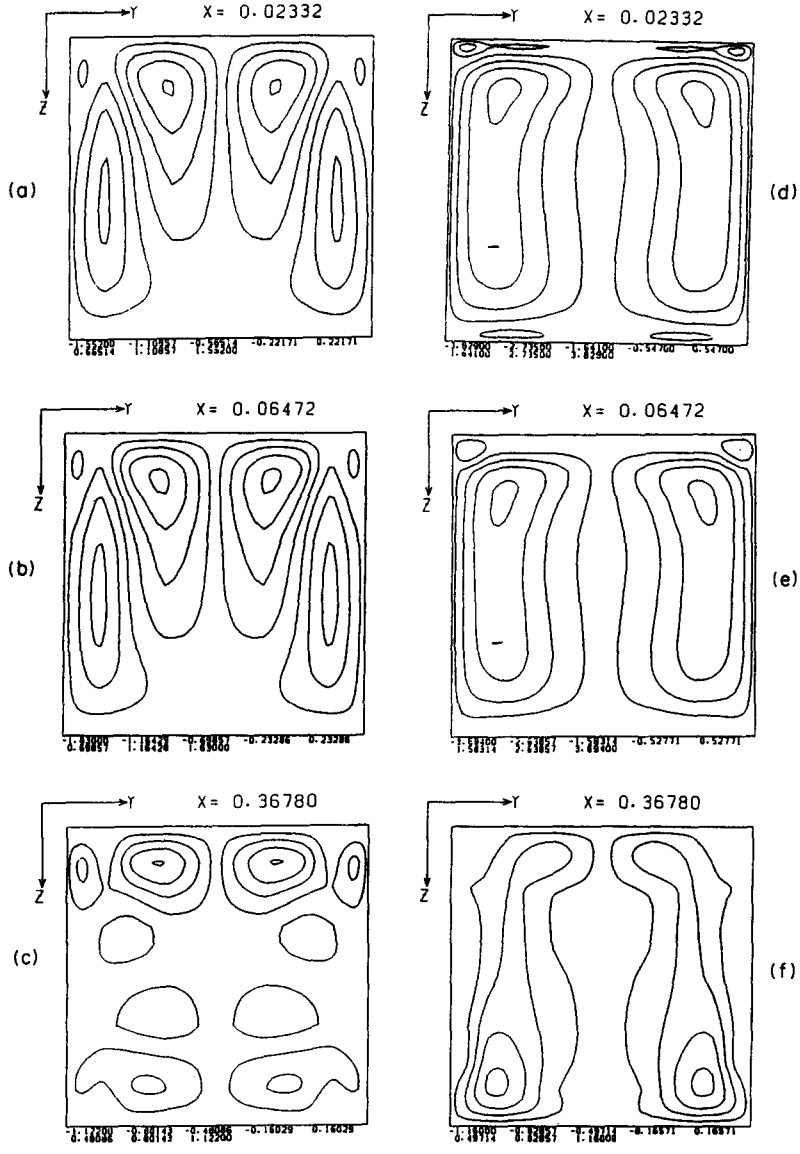

FIG. 11. Contour maps of vector potential Ψ_x at $Ra = 10^6$ and $Pr = 0.054$: (a) at $Ha = 0$ and $X = 0.023$; (b) at $Ha = 0$ and $X = 0.0647$; (c) at $Ha = 0$ and $X = 0.3678$; (d) at $Ha = 300$ and $X = 0.023$; (e) at $Ha = 300$ and $X = 0.0647$; (f) at $Ha = 300$ and $X = 0.3678$.

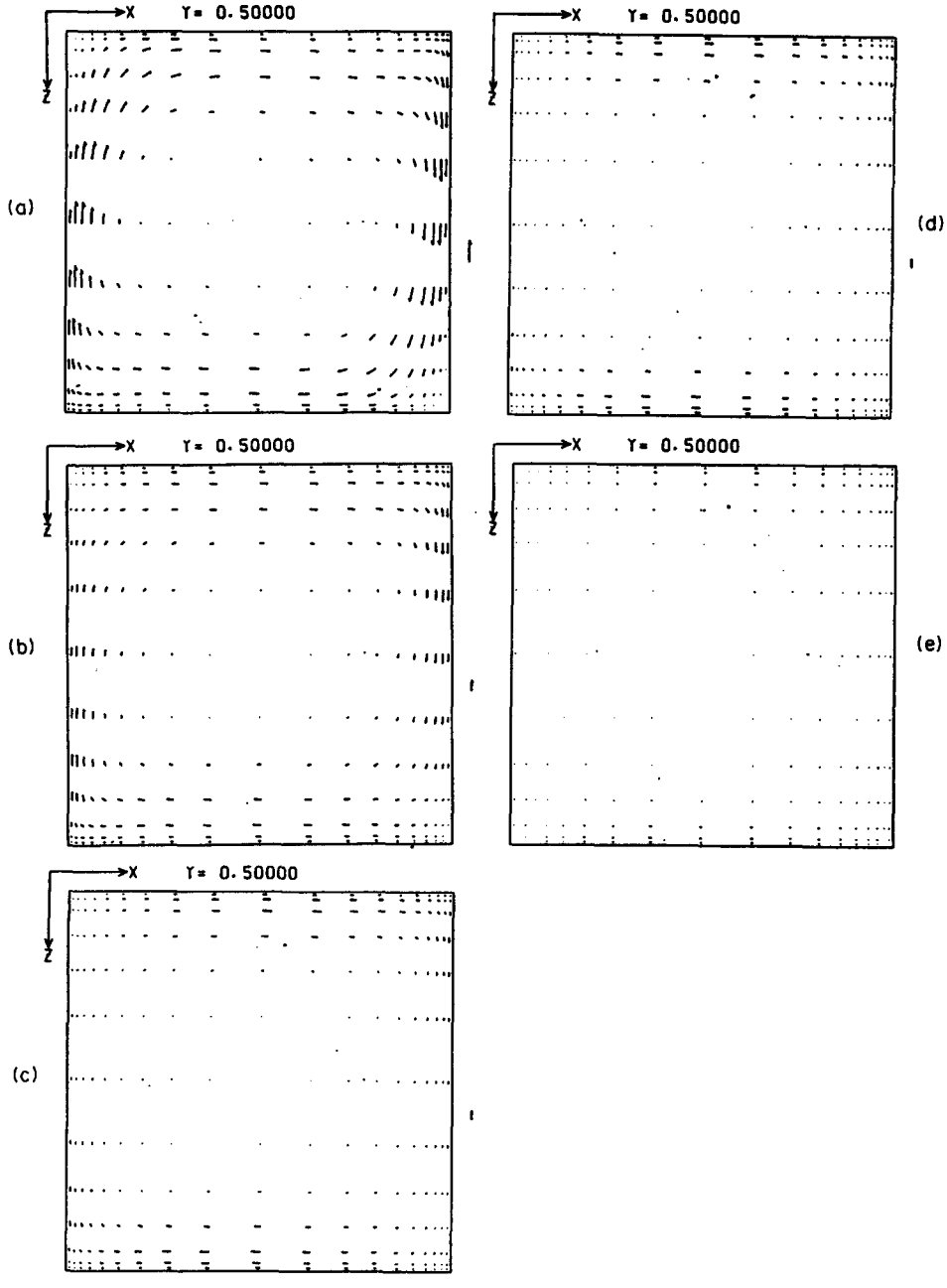

FIG. 12. Velocity vectors at $Y = 0.5$ under various strengths of the magnetic field in the X-direction at $Ra = 10^6$ and $Pr = 0.054$: (a) $Ha = 0$; (b) $Ha = 100$; (c) $Ha = 200$; (d) $Ha = 300$; (e) $Ha = 500$.

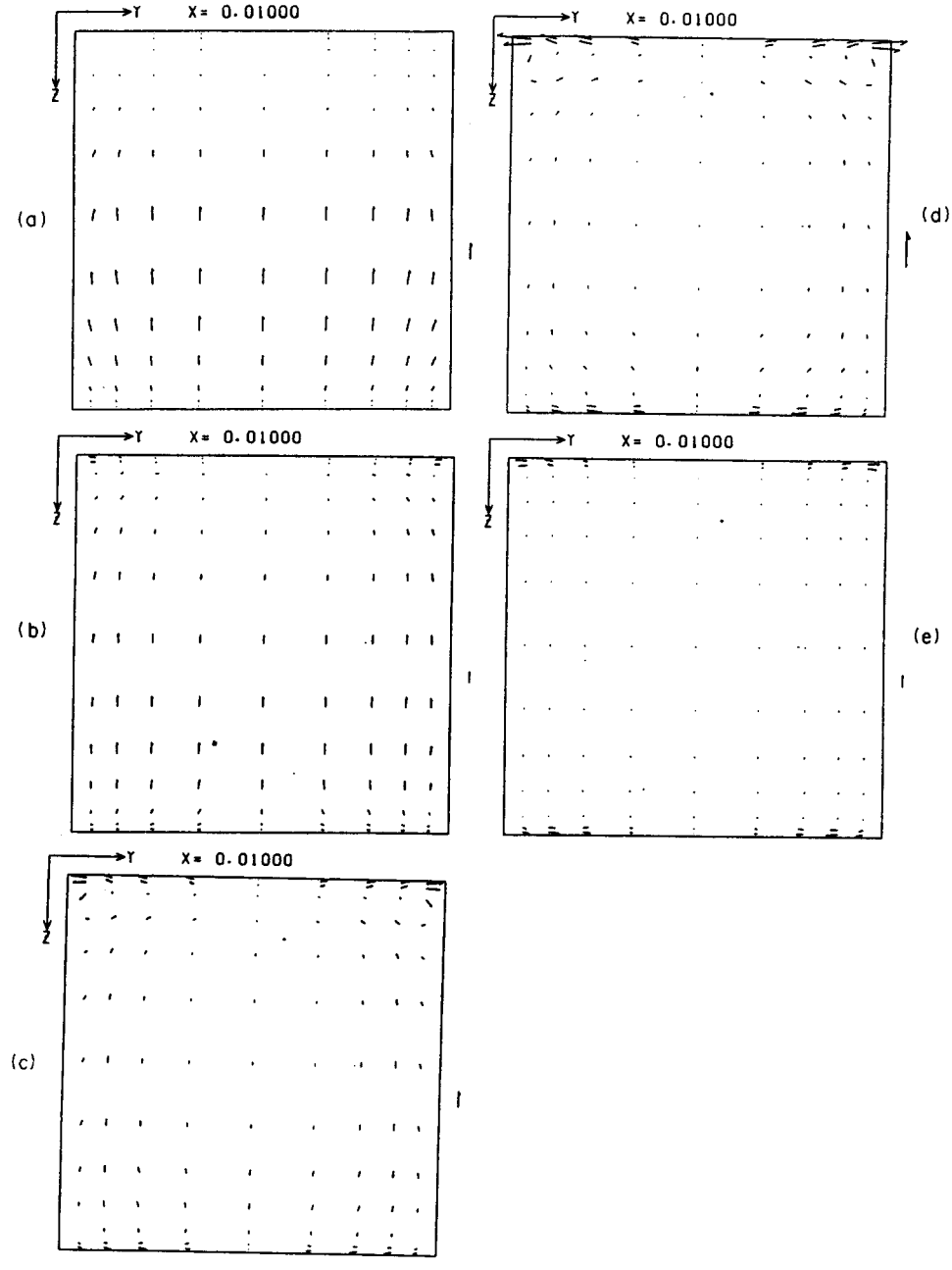

FIG. 13. Velocity vectors at $X = 0.01$ under various strengths of the magnetic field in the X-direction at $Ra = 10^6$ and $Pr = 0.054$: (a) $Ha = 0$; (b) $Ha = 100$; (c) $Ha = 200$; (d) $Ha = 300$; (e) $Ha = 500$.

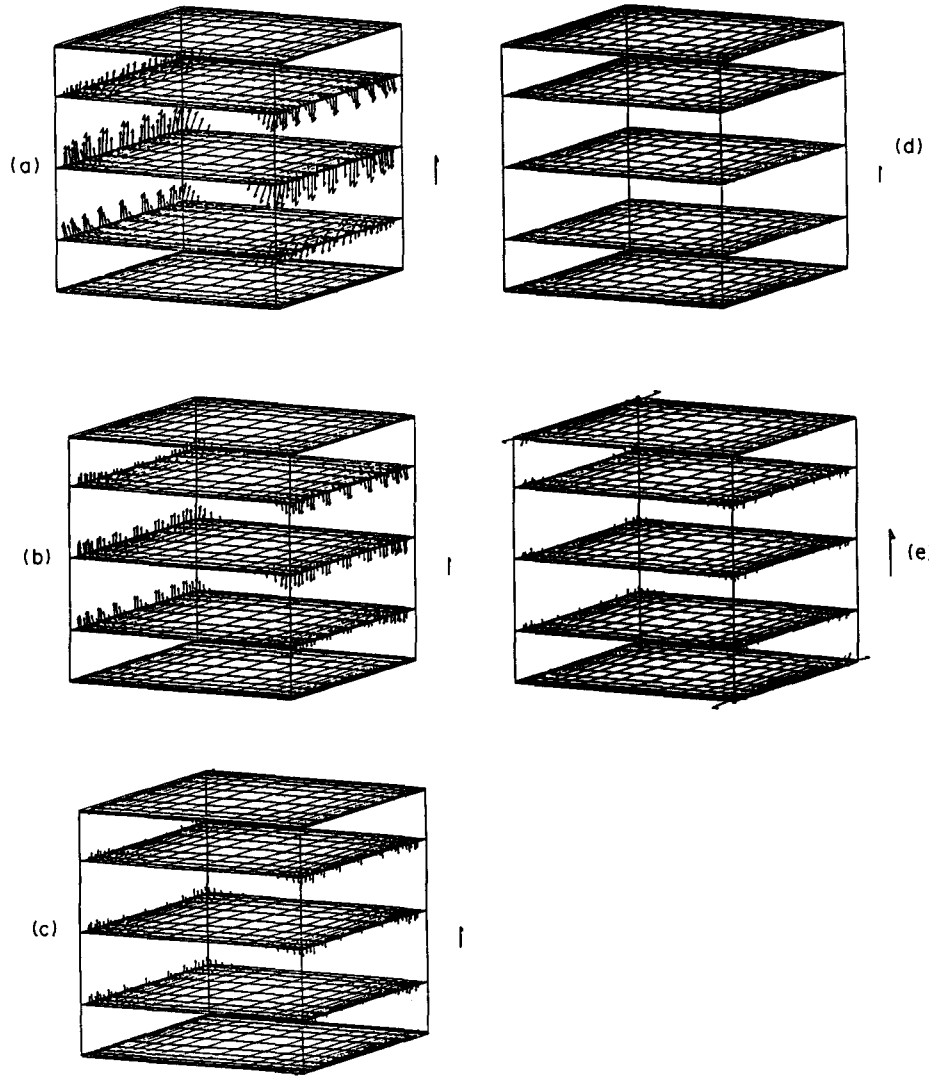

FIG. 14. Perspective view of velocity vectors at $Ra = 10^6$ and $Pr = 0.054$: (a) $Ha = 0$; (b) $Ha = 100$; (c) $Ha = 200$; (d) $Ha = 300$; (e) $Ha = 500$.

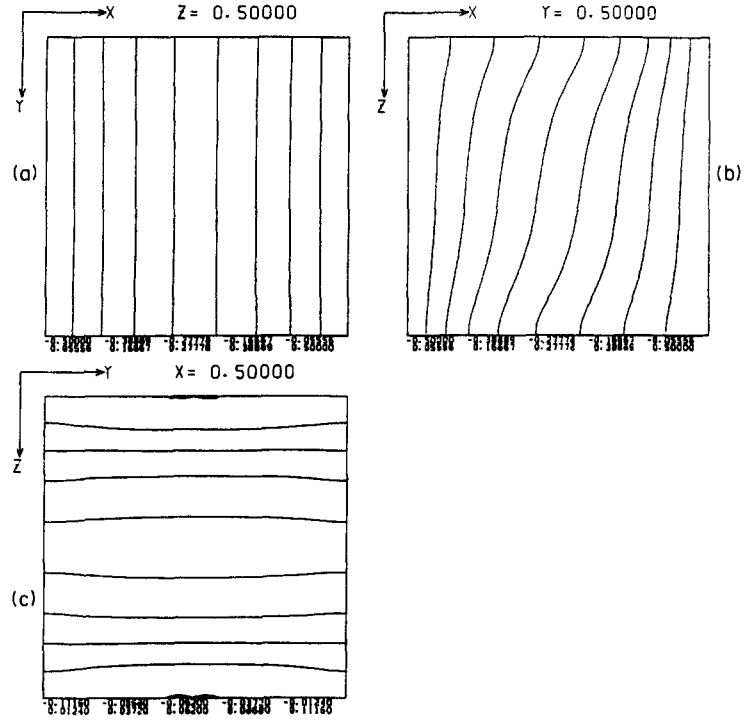

FIG. 15. Isothermal lines at $Ra = 10^6$, $Pr = 0.054$ and $Ha = 500$: (a) at $Z = 0.5$; (b) at $Y = 0.5$; (c) at $X = 0.5$.

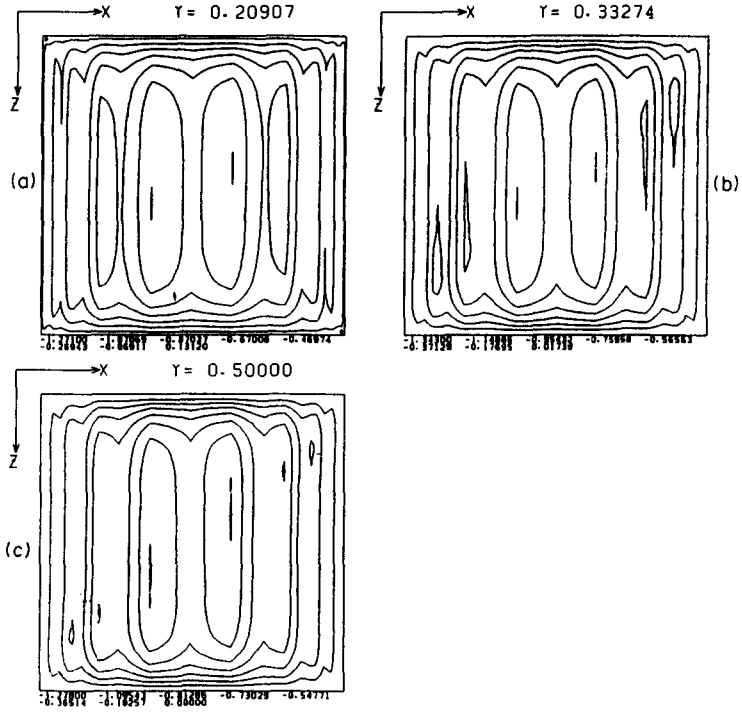

FIG. 16. Contour maps of vector potential Ψ_y at $Ra = 10^6$, $Pr = 0.054$ and $Ha = 500$: (a) $Y = 0.21$; (b) $Y = 0.33$; (c) $Y = 0.5$.

but parallel to the vertical heated wall was found to be least effective in suppressing the circulation flow. The external magnetic field in the vertical direction was found to be effective in between these two extremes.

For the sample calculations at $Ra = 10^6$, $Ha = 300$ and $Pr = 0.054$, the main circulation was suppressed by the magnetic field (X-direction) but the secondary flow became stronger than those for no magnetic field. Under this condition, the peculiar diverging flow was found to exist at the upper corners of the vertical heated wall and at the lower corners of the cooled vertical wall.

REFERENCES

1. K. Hoshi, N. Izawa and T. Suzuki, Growth of single crystal in a magnetic field—silicon, *Appl. Phys.* (in Japanese) **53,** 38–41 (1984).
2. R. Hunt and G. Wilks, Low Prandtl number magneto-hydrodynamic natural convection in a strong cross field, *Numer. Heat Transfer* **4,** 303–316 (1981).
3. M. Nagase, O. Takahashi, I. Michiyoshi and N. Takenaka, Heat transfer by natural convection of liquid metal in a magnetic field, *Prepr. 22nd Nat. Heat Transfer Symp., Japan* (in Japanese) **C304,** 413–415 (1985).
4. P. Tabeling, Convective flow patterns in rectangular boxes of finite extent under an external magnetic field, *J. Physique* **43,** 1295–1303 (1982).
5. A. Raptis and J. Vlahos, Unsteady hydromagnetic free convective flow through a porous medium, *Lett. Heat Mass Transfer* **9,** 59–64 (1982).
6. T. Maekawa and I. Tanasawa, The effects of gravitational and magnetic field on the Marangoni convection in a horizontal fluid layer, *Prepr. 23rd Nat. Heat Transfer Symp., Japan* (in Japanese) **C221,** 391–393 (1986).
7. T. Munakata and I. Tanasawa, Effect of external magnetic field on natural convection during crystal growth process from melt, *Prepr. 24th Nat. Heat Transfer Symp., Japan* (in Japanese) **B321,** 281–283 (1987).
8. N. O. Weiss, Convection in an imposed magnetic field, Part 1. The development of nonlinear convection, *J. Fluid Mech.* **108,** 247–272 (1981).
9. H. Ozoe and E. Maruo, Magnetic and gravitational natural convection of melted silicon—two-dimensional numerical computations for the rate of heat transfer, *JSME Int.* **30,** 774–784 (1987).
10. M. Michelcic, K. Wingerath and Chu. Pirron, Three-dimensional simulations of the Czochralski bulk flow, *J. Crystal Growth* **69,** 473–488 (1984).
11. T. Maekawa and I. Tanasawa, Convective instability of hydromagnetic liquid driven by Marangoni effect, *Prepr. 22nd Nat. Heat Transfer Symp., Japan* (in Japanese) **C303,** 410–412 (1985).
12. S. Kobayashi, Effect of an external magnetic field on solute distribution in Czochralski grown crystals—a theoretical analysis, *J. Crystal Growth* **75,** 301–308 (1986).
13. H. Ozoe, A. Mouri, M. Hiramitsu, S. W. Churchill and N. Lior, Numerical calculation of three-dimensional turbulent natural convection in a cubical enclosure using a two-equation model for turbulence, *J. Heat Transfer* **108,** 806–813 (1986).
14. G. J. Hirasaki and J. D. Hellums, A general formulation of the boundary conditions on the vector potential in three-dimensional hydrodynamics, *Q. Appl. Math.* **26,** 331–342 (1968).

EFFET DE LA DIRECTION D'UN CHAMP MAGNETIQUE EXTERNE SUR LA CONVECTION NATURELLE TRIDIMENSIONNELLE DANS UNE ENCEINTE CUBIQUE

Résumé—Les équations tridimensionnelles de conservation pour la convection naturelle dans une enceinte cubique chauffée sur un côté et refroidie sur la paroi opposée sont résolues numériquement pour trois champs magnétiques externes différents agissant dans chacune des directions X, Y ou Z. Des exemples de calcul sont conduits pour $Ra = 10^6$ et 10^7, $Ha = 0$–500, $Pr = 0{,}054$. Le champ magnétique perpendiculaire à l'écoulement vertical du type couche limite est le plus efficace pour supprimer la convection. Le champ parallèle aux parois verticales chaude et froide est le moins efficace, bien qu'il soit perpendiculaire à la circulation principale du fluide le long des frontières verticale ou horizontale. Quand le champ est augmenté, par exemple, à $Ra = 10^6$ et $Ha = 300$, l'écoulement secondaire est deux fois plus important avec une réduction de l'écoulement principal de circulation.

DER EINFLUSS DER RICHTUNG EINES ÄUSSEREN MAGNETFELDES AUF DIE DREIDIMENSIONALE NATÜRLICHE KONVEKTION IN EINEM WÜRFELFÖRMIGEN HOHLRAUM

Zusammenfassung—Die dreidimensionalen Gleichungen für natürliche Konvektion in einem Würfel, bei dem eine Seitenwand gekühlt und die gegenüberliegende beheizt wird, werden numerisch gelöst. In die Lösung wird ein außen angelegtes Magnetfeld einbezogen, dessen Richtungsvektor in X-, Y- oder Z-Richtung verläuft. Die Berechnungen werden für $Ra = 10^6$ und 10^7 durchgeführt mit $Pr = 0{,}054$ und $Ha = 0$ bis 500. Wenn der Richtungsvektor des außen angelegten Magnetfeldes senkrecht zur vertikalen Grenzschichtströmung verläuft, ist die Konvektionsunterdrückung am besten. Wenn das Magnetfeld allerdings parallel zur senkrechten Heiz- bzw. Kühlwand verläuft, ist die Konvektionsunterdrückung am geringsten, obwohl das Feld dann senkrecht zur Hauptströmungsrichtung an den senkrechten und waagerechten Wänden verläuft. Wenn das Magnetfeld stark ist z. B. bei $Ra = 10^6$ und $Ha = 300$, wird die Sekundärströmung doppelt so stark und die Hauptströmung verlangsamt.

ВЛИЯНИЕ НАПРАВЛЕНИЯ ВНЕШНЕГО МАГНИТНОГО ПОЛЯ НА ТРЕХМЕРНУЮ ЕСТЕСТВЕННУЮ КОНВЕКЦИЮ В КУБИЧЕСКОЙ ПОЛОСТИ

Аннотация—Численно решаются трехмерные уравнения, описывающие естественную конвекцию в кубической полости, одна из боковых стенок которой нагревается, а противоположная охлаждается, в трех различных внешних магнитных полях, направленных вдоль одной из осей: X, Y или Z. Выполнены пробные расчеты для $Ra = 10^6$ и 10^7, а также для $Ha = 0$–500 при $Pr = 0{,}054$. Найдено, что внешнее магнитное поле, направленное перпендикулярно течению в вертикальном пограничном слое, наиболее сильно подавляет конвекцию. Однако внешнее магнитное поле, параллельное вертикальным нагретой и холодной стенкам, минимально подавляет ее, хотя и направлено перпендикулярно основному течению, циркулирующему вдоль вертикальной и горизонтальной границ. При относительном усилении магнитного поля, например, когда $Ra = 10^6$ и $Ha = 300$, найдено, что интенсивность вторичного течения возрастает вдвое с уменьшением интенсивности основного течения.